PHYSICAL REVIEW D **79,** 045026 (2009)

Cosmological constraints on a light nonthermal sterile neutrino

Mario A. Acero[1,2,3] and Julien Lesgourgues[4,5]

[1]*Dipartimento di Fisica Teorica, Università di Torino, Via P. Giuria 1, I–10125 Torino, Italy*
[2]*INFN, Sezione di Torino, Via P. Giuria 1, I–10125 Torino, Italy*
[3]*Laboratoire d'Annecy-le-Vieux de Physique Thórique LAPTH, Université de Savoie, CNRS/IN$_2$P$_3$, 74941 Annecy-le-vieux, France*
[4]*PH-TH, CERN—CH-1211 Geneva 23, Switzerland*
[5]*SB-ITP-LPPC, BSP 312—EPFL, CH-1015 Lausanne, Switzerland*

(Received 17 December 2008; published 27 February 2009)

Although the MiniBooNE experiment has severely restricted the possible existence of light sterile neutrinos, a few anomalies persist in oscillation data, and the possibility of extra light species contributing as a subdominant hot (or warm) component is still interesting. In many models, this species would be in thermal equilibrium in the early universe and share the same temperature as active neutrinos, but this is not necessarily the case. In this work, we fit up-to-date cosmological data with an extended ΛCDM model, including light relics with a mass typically in the range 0.1–10 eV. We provide, first, some nearly model-independent constraints on their current density and velocity dispersion, and second, some constraints on their mass, assuming that they consist either in early decoupled thermal relics, or in nonresonantly produced sterile neutrinos. Our results can be used for constraining most particle-physics-motivated models with three active neutrinos and one extra light species. For instance, we find that at the 3σ confidence level, a sterile neutrino with mass $m_s = 2$ eV can be accommodated with the data provided that it is thermally distributed with $T_s/T_\nu^{\rm id} \lesssim 0.8$ or nonresonantly produced with $\Delta N_{\rm eff} \lesssim 0.5$. The bounds become dramatically tighter when the mass increases. For $m_s \lesssim 0.9$ eV and at the same confidence level, the data is still compatible with a standard thermalized neutrino.

DOI: 10.1103/PhysRevD.79.045026 PACS numbers: 14.60.Pq, 98.80.Cq

I. INTRODUCTION

Neutrino oscillation is a well-studied phenomenon, confirmed by strong experimental evidences. Most experimental results are well explained with a three-neutrino oscillation model, involving two independent and well-measured square-mass differences: $\Delta m^2_{\rm sol} = (7.59 \pm 0.21) \times 10^{-5}$ eV^2 [1] and $\Delta m_{\rm atm} = (2.74^{+0.44}_{-0.26}) \times 10^{-3}$ eV^2 [2] (a recent global fit to data from solar, atmospheric, reactor, and accelerator experiments gives the best-fit values $\Delta m^2_{21} = (7.65^{+0.23}_{-0.20}) \times 10^{-5}$ eV^2 and $|\Delta m_{31}| = (2.40^{+0.12}_{-0.11}) \times 10^{-3}$ eV^2 [3,4]). However, some other experiments have shown some anomalies which do not fit in this hypothesis (Liquid Scintillator Neutrino Detector (LSND) [5], Gallium experiments [6], MiniBooNE low energy anomaly [7]). These anomalous results might be due to unknown systematic effects, but all attempts to identify such systematics have failed until now. Otherwise, they could be interpreted as exotic neutrino physics.

In Ref. [8], the MiniBooNE anomaly was explained through a renormalization of the absolute neutrino flux and a simultaneous disappearance of electron neutrinos oscillating into sterile neutrinos (with $P_{\nu_e \to \nu_e} = 0.64^{+0.08}_{-0.07}$). The LSND and Gallium radioactive source experiment [9–11] anomalies have been studied in Ref. [12], where is it claimed that all these anomalies could be interpreted as an indication of the presence of, at least, one sterile neutrino with rather large mass (few eV's). Reference [13] also studied the compatibility of the Gallium results with the Bugey [14] and Chooz [15] reactor experimental data, concluding that such a sterile neutrino should have a mass between 1 and 2 eV's. Finally, the MiniBooNE collaboration performed global fits of MiniBooNE, LSND, KARMEN2, and Bugey experiments in the presence of a fourth sterile neutrino [16] (assuming no renormalization issue for MiniBooNe unlike Ref. [8]). When all four experiments are combined, the compatibility between them is found to be very low (4%); however, when only three of them are included, the compatibility level is usually reasonable (the largest tension being found between LSND and Bugey). In this analysis, the preferred value of the sterile neutrino is usually smaller than 1 eV, but still of possible cosmological relevance (for instance, for all four experiments, the best-fit corresponds to $\Delta m^2 \sim 0.2$–0.3 eV^2).

Models with more than one sterile neutrino (with eV-scale masses) have also been considered as a possible way of accommodating the LSND and MiniBooNE data. For instance, the authors of Ref. [17] found that a (3 + 2) scheme (3 standard active neutrinos plus 2 sterile neutrinos) provides a good fit to LSND and MiniBooNE, although there is a tension between appearance (LSND, MiniBooNE, KARMEN, NOMAD) and disappearance (Bugey, Chooz, Palo Verde, CDHS) experimental data. In the same reference, it was found that a

(3 + 3) scheme does not bring anything new with respect to the (3 + 2) case; in particular, the conflict between appearance and disappearance experimental data remains.

These various developments suggest that it is important to scrutinize cosmological bounds on scenarios with one light sterile neutrino, which could help ruling them out, given that current bounds on the total neutrino mass assuming just three active neutrinos are as low as $\sum m_\nu < 0.61$ eV (using WMAP5, baryon acoustic oscillations (BAO), and SN data [18]). This result cannot be readily applied to the models which we consider here. Indeed, scenarios with extra neutrinos require a specific cosmological analysis, for the simple reason that besides affecting the total neutrino mass, additional neutrinos also increase the abundance of relativistic particles in the early universe.

From the point of view of cosmology, there have been many works constraining simultaneously the sum of neutrino masses and the contribution to the relativistic energy density component of the Universe, parametrized as the effective number of neutrinos, $N_{\rm eff}$ (see for example [19–24]). Most of these works assume either that the heaviest neutrino (and hence the most relevant one from the point of view of free-streaming) has a thermal distribution, sharing the same value of temperature as active neutrinos, or that all neutrinos are degenerate in mass. However, the results of Refs. [25,26] can also be applied to the case of very light active neutrinos plus one heavier, non-necessarily thermal sterile neutrino, which is the most interesting case for explaining oscillation anomalies. In terms of physical motivations, it is very likely that the light sterile neutrino required by the LSND anomaly acquires a thermal distribution in the early universe, through oscillations with active neutrinos in the presence of a large mixing angle [27]. On the other hand, there are some proposals to avoid these constraints (for a list of some scenarios, see [28]). One of such possibilities is based on a low reheating temperature (T_R) universe [29–33], in which, for a sufficiently low T_R, the sterile neutrinos could be nonthermal [34] and its production would be suppressed [31], such that usual cosmological bounds are evaded. In fact, in these models, sterile neutrinos are allowed to have a large mass without entering in conflict with other experimental results, while $T_{\rm dec} \lesssim T_R \lesssim 10$ MeV ($T_{\rm dec}$ being the temperature of the cosmic plasma at neutrino decoupling).

In the absence of thermalization, cosmological bounds on the sterile neutrino mass become potentially weaker. Hence, it is interesting to study the compatibility of recently proposed scenarios with a light sterile neutrino with the most recent cosmological data, keeping in mind the possibility of a nonthermal distribution. The goal of this paper is hence to study the compatibility of cosmological experimental data (WMAP5 plus small-scale cosmic microwave background (CMB) data, Sloan Digital Sky Survey luminous red galaxies (SDSS LRG) data, SNIa data from Supernovae Legacy Survey (SNLS) and conservative Lya data from VISTA Hemisphere Survey (VHS)) with the hypothesis of a sterile neutrino with the characteristics sketched above, i.e., with a mass roughly of the order of the electron Volt, and a contribution to $N_{\rm eff}$ smaller than one.

II. LIGHT STERILE NEUTRINO IN COSMOLOGY: PHYSICAL EFFECTS AND PARAMETRIZATION

If a population of free-streaming particles becomes nonrelativistic after photon decoupling, its physical effects on the cosmological background and perturbation evolution are mainly described by three quantities:

(1) its contribution to the relativistic density before photon decoupling, which affects the redshift of radiation/matter equality, usually parametrized by an effective neutrino number (standing for the relativistic density of the species divided by that of one massless neutrino family in the instantaneous decoupling (id) limit):

$$\Delta N_{\rm eff} \equiv \frac{\rho_s^{\rm rel}}{\rho_\nu} = \left[\frac{1}{\pi^2}\int dp\, p^3 f(p)\right] \Big/ \left[\frac{7}{8}\frac{\pi^2}{15} T_\nu^{\rm id\,4}\right] \tag{1}$$

with $T_\nu^{\rm id} \equiv (4/11)^{1/3} T_\gamma$,

(2) its current energy density, which affects (i) the current energy budget of the Universe (with various consequences for the CMB and large scale structures (LSS) spectra, depending on which other parameters are kept fixed), and (ii) the amplitude reduction in the small-scale matter power spectrum due to these extra massive free-streaming particles, parametrized by the dimensionless number ω_s:

$$\omega_s \equiv \Omega_s h^2 = \left[\frac{m}{\pi^2}\int dp\, p^2 f(p)\right] \times \left[\frac{h^2}{\rho_c^0}\right], \tag{2}$$

where ρ_c^0 is the critical density today and h the reduced Hubble parameter,

(3) the comoving free-streaming length of these particles when they become nonrelativistic, which controls the scale at which the suppression of small-scale matter fluctuations occurs. This length can easily be related to the average velocity of the particles today, $\langle v_s \rangle$.[1]

[1]The minimum comoving free-streaming wave number $k_{\rm fs}$ is controlled by Ω_m and by the ratio $a(t_{\rm nr})/\langle v_s(t_{\rm nr})\rangle$ evaluated when $T = m$, i.e. when $a(t_{\rm nr}) \sim \langle v_s(t_0)\rangle a(t_0)$. Given that $\langle v_s(t_{\rm nr})\rangle \sim \langle v_s(t_0)\rangle a(t_0)/a(t_{\rm nr})$, the minimum comoving free-streaming length just depends on $\langle v_s(t_0)\rangle$ and Ω_m.

However, for whatever assumption concerning the phase-space distribution function $f(p)$, the three numbers $(\Delta N_{\rm eff}, \omega_s, \langle v_s \rangle)$ satisfy a constraint equation. Indeed, the average velocity of the particles today (assumed to be in the nonrelativistic regime) is given *exactly* by

$$\langle v_s \rangle \equiv \frac{\int p^2 dp \frac{p}{m} f(p)}{\int p^2 dp f(p)} = \frac{7}{8}\frac{\pi^2}{15}\left(\frac{4}{11}\right)^{4/3}\frac{T_{\rm CMB}^4 h^2}{\rho_c}\frac{\Delta N_{\rm eff}}{\omega_s} = 5.618 \times 10^{-6}\frac{\Delta N_{\rm eff}}{\omega_s} \tag{3}$$

in units where $c = k_B = \hbar = 1$, and taking $T_{\rm CMB} = 2.726$ K. Hence, the three physical effects described above depend on only *two independent parameters*.

Reducing the physical impact of any population of massive free-streaming particles to these three effects (and two independent parameters) is a simplification: two models based on different nonthermal phase-space distributions $f(p)$ can in principle share the same numbers $(\Delta N_{\rm eff}, \omega_s, \langle v_s \rangle)$ and impact the matter power spectrum differently. Indeed, the free-streaming effect depends on the details of $f(p)$ (including high statistical momenta like $\int dp\, p^4 f(p)$, etc.) However, the conclusions of Ref. [21] indicate that for many models with nonthermal distortions, observable effects can indeed be parametrized by two combinations of $(\Delta N_{\rm eff}, \omega_s, \langle v_s \rangle)$ with good accuracy: other independent parameters would be very difficult to observe.[2]

Let us compute the three parameters $(\Delta N_{\rm eff}, \omega_s, \langle v_s \rangle)$ for simple cases. For one species of thermalized free-streaming particles with mass m_s, sharing the same temperature as active neutrinos in the instantaneous decoupling limit, one gets

$$\Delta N_{\rm eff} = 1, \qquad \omega_s = \frac{m_s}{94.05\ {\rm eV}}, \qquad \langle v_s \rangle = \frac{7\pi^4}{180\zeta(3)}\frac{T_\nu^{\rm id}}{m_s} = \frac{0.5283\ {\rm meV}}{m_s}. \tag{4}$$

For a light thermal relic with a Fermi-Dirac distribution and a different temperature T_s, these quantities become

$$\Delta N_{\rm eff} = \left(\frac{T_s}{T_\nu^{\rm id}}\right)^4, \qquad \omega_s = \frac{m_s}{94.05\ {\rm eV}}\left(\frac{T_s}{T_\nu^{\rm id}}\right)^3, \qquad \langle v_s \rangle = \frac{0.5283\ {\rm meV}}{m_s}\left(\frac{T_s}{T_\nu^{\rm id}}\right). \tag{5}$$

For a nonthermal relic with a free function $f(p)$, there is an infinity of possible models. A popular one is the Dodelson-Widrow (DW) scenario [36] (also referred to as the "nonresonant production scenario"), motivated by early active-sterile neutrino oscillations in the limit of the small mixing angle and zero leptonic asymmetry, which corresponds to the phase-space distribution

$$f(p) = \frac{\chi}{e^{p/T_\nu} + 1}, \tag{6}$$

where χ is an arbitrary normalization factor. In this case, in the approximation $T_\nu = T_\nu^{\rm id}$, the three "observable" parameters read

$$\Delta N_{\rm eff} = \chi, \qquad \omega_s = \frac{m_s}{94.05\ {\rm eV}}\chi, \qquad \langle v_s \rangle = \frac{0.5283\ {\rm meV}}{m_s}. \tag{7}$$

Hence, a Dodelson-Widrow model shares the same observable parameters $(\Delta N_{\rm eff}, \omega_s, \langle v_s \rangle)$ as a thermal model with $m_s^{\rm thermal} = m_s^{\rm DW}\chi^{1/4}$ and $T_s = \chi^{1/4} T_\nu$. Actually, for these two models, the degeneracy is exact: it can be shown by a change of variable in the background and linear perturbation equations that the two models are strictly equivalent from the point of view of cosmological observables [21,37]. As mentioned before, in the general case, two models sharing the same $(\Delta N_{\rm eff}, \omega_s, \langle v_s \rangle)$ are not always strictly equivalent, but can be thought to be hardly distinguishable even with future cosmological data. For instance, the low-temperature reheating model analyzed in [30,31] leads to a distribution of the form

$$f(p) = \frac{\chi p}{e^{p/T_\nu} + 1}. \tag{8}$$

This model would in principle deserve a specific analysis, but in good approximation we can expect that by only exploring the parameter space of thermal models (or equivalently, of DW models), we will obtain some very generic results, covering in good approximation most possibilities for the nonthermal distortions.

III. ANALYSIS

A. Data

In the following sections, we will present the results of various runs based on the Boltzmann code CAMB [38] and cosmological parameter extraction code COSMOMC [39].

[2]This conclusion does not apply when the nonthermal distribution $f(p)$ has a sharp peak close to $p = 0$. In this case, particles with very small momentum should be counted within the CDM component, not within the extra massive free-streaming component. Otherwise, one would obtain values of ω_s and $\langle v_s \rangle$ based on an average between cold and hot/warm particles; then, these parameters would not capture the correct physical effects (see [35]).

We modified CAMB in order to implement the proper phase-space distribution $f(p)$ of the thermal or DW model. For simplicity, we assumed in all runs that the three active neutrinos can be described as massless particles.[3] In order to obtain a Bayesian probability distribution for each cosmological parameter, we ran COSMOMC with flat priors on the usual set of six parameters ω_b, $\omega_{\rm dm} = \omega_s + \omega_{\rm cdm}$, θ, τ, A_s, n_s (see e.g. [40]), plus two extra parameters describing the sterile neutrino sector, that will be described in the next sections. We choose the following data set: WMAP5 [41] plus small-scale CMB data (ACBAR [42], CBI [43], Boomerang [44]), the galaxy power spectrum of the SDSS LRG [45] with flat prior on Q [46,47], SNIa data from SNLS [48], and conservative Lyman-α data from VHS [49]. We do not include more recent Lyman-α data sets, which have much smaller error bars, but for which the deconvolution of nonlinear effects depends on each particular cosmological model and requires specific hydrodynamical simulations.

B. General analysis

Our first goal is to obtain simple results with a wide range of applications. Hence, we should not parametrize the effect of sterile neutrinos with e.g. their mass or temperature: in that case, our results would strongly depend on underlying assumptions for $f(p)$. It is clear from Sec. II that nearly "universal" results can be obtained by employing two combinations of the "observable parameters" $\Delta N_{\rm eff}$, ω_s, and $\langle v_s \rangle$ (and eventually of other parameters of the ΛCDM model). Here we choose to vary the current dark matter density fraction $f_s = \omega_s/(\omega_s + \omega_{\rm cdm})$ and the current velocity dispersion $\langle v_s \rangle$. As will be clear from our results, these two parameters capture the dominant observable effects, and lead to very clear bounds, since their correlation with other ΛCDM model parameters is insignificant. Our limits on f_s and $\langle v_s \rangle$ apply exactly to the thermal case and DW case and approximately to most other cases (modulo the caveat described in the second footnote of Sec. II).

Our parameter space is represented in Fig. 1. We adopt a logarithmic scale for $\langle v_s \rangle$ and display the interesting range

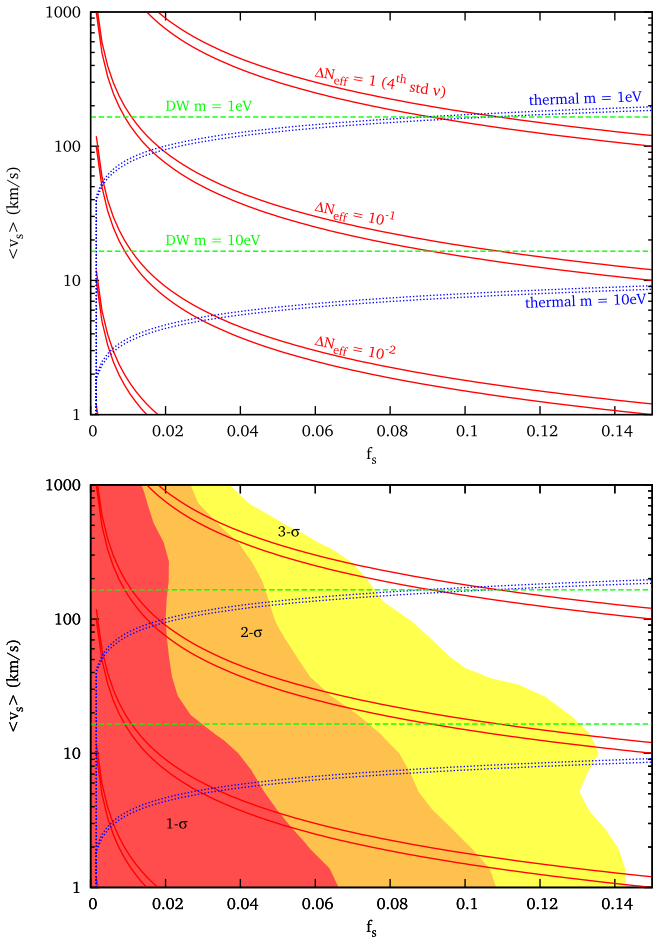

FIG. 1 (color online). (Top) The parameter space $(f_s, \langle v_s \rangle)$ chosen in our general analysis. The thin bands delimited by red/solid lines show regions of equal $\Delta N_{\rm eff}$ (assuming $\omega_{\rm dm} = 0.11 \pm 0.01$); these bands are fully model independent. We also show the model-dependent regions of equal mass, delimited by blue/dotted lines for the case of early decoupled thermal relics, and consisting in horizontal green/dashed lines for Dodelson-Widrow sterile neutrinos. (Bottom) Same with, in addition, the regions allowed at the 68.3% (1σ), 95.4% (2σ), and 99.7% (3σ) C.L. by our cosmological data set, in a Bayesian analysis with flat priors on f_s and $\log_{10}\langle v_s \rangle$ within the displayed range.

$$1\ {\rm km/s} < \langle v_s \rangle < 1000\ {\rm km/s}. \tag{9}$$

Indeed, with out data set, particles with smaller velocities would be indistinguishable from cold dark matter; instead, particles with larger velocities would either have $\Delta N_{\rm eff} > 1$ (a case beyond the motivations of this work, and anyway very constrained by the data) or $f_s < 0.02$ (being indistinguishable from extra relativistic degrees of freedom). Assuming a particular value for $\omega_{\rm dm} = \omega_s + \omega_{\rm cdm}$ and for $\Delta N_{\rm eff}$, it is possible to compute the velocity dispersion $\langle v_s \rangle$ as a function of f_s. Since the CMB and LSS data give precise constraints on $\omega_{\rm dm}$, regions of equal $\Delta N_{\rm eff}$ correspond to thin bands in the $(f_s, \langle v_s \rangle)$ plane. We show these bands in Fig. 1 for $10^{-3} < \Delta N_{\rm eff} < 1$ under the assumption

[3] In principle, this is not a good assumption, since data from neutrino oscillations provide a lower bound on the total mass of active neutrinos, roughly $\sum m_\nu^{\rm active} \geq |\Delta m_{31}|^{1/2}$, corresponding to $\omega_\nu^{\rm active} \geq 5 \times 10^{-4}$. However, as long as we consider sterile neutrinos with $\omega_s \gg \omega_\nu^{\rm active}$, the effect of active neutrino masses on the CMB and LSS spectra is overseeded by that of sterile neutrinos, and our approximation is sufficient. If active neutrinos masses are degenerate with $\sum m_\nu^{\rm active} \sim 1$ eV and $\omega_\nu^{\rm active} \sim 10^{-2}$ (larger values are disfavored by cosmological data), they could partially modify our results, especially in the region in parameter space where $f_s \leq 0.1$. However, if active neutrinos obey to a hierarchical or inverted hierarchical mass splitting, our results are essentially unaffected by this approximation, since in the various cases considered thereafter, most of the relevant parameter space corresponds to $f_s \gg 10^{-2}$ and hence $\omega_s \gg \omega_\nu^{\rm active}$.

that $\omega_{\rm dm} = 0.11 \pm 0.01$, which corresponds roughly to the 95% confidence limits (C.L.) from all our runs. These iso-$\Delta N_{\rm eff}$ bands are completely model independent.

Instead, regions of equal mass can only be plotted for a particular model. In Fig. 1, we show the bands corresponding to $m = 1$ eV and 10 eV, either in the case of early decoupled thermal relics (blue/dotted lines) or in the DW case (green/dashed lines). For any given mass, these bands intersect each other in a location corresponding to the case of one-fourth standard neutrino species with $\Delta N_{\rm eff} = 1$.

We ran COSMOMC with top-hat priors on f_s (in the physical range [0, 1]) and on $\log_{10}[\langle v_s\rangle/1\ {\rm km/s}]$ (in the range [0, 3] motivated by the previous discussion). Our results are summarized in Fig. 1 (bottom). We see that the upper bound on f_s decreases smoothly as the velocity dispersion increases: when the particles have a larger velocity dispersion, their free-streaming wavelength is larger, so the steplike suppression in the power spectrum (which amplitude depends on f_s) is more constrained. For $\langle v_s\rangle \sim 1$ km/s, we find $f_s \lesssim 0.1$ at the 2σ C.L., while for $\langle v_s\rangle \sim 100$ km/s, we find $f_s \lesssim 0.06$ at the 2σ C.L. When the velocity dispersion becomes larger than 100 km/s, the upper bound on f_s decreases even faster as a function of $\langle v_s\rangle$. This is the case of a hot dark matter (HDM) component with significant contribution to the number of relativistic degrees of freedom, for which the observational bounds derive from a combination of the first and second effects described in Sec. II: in this limit, in addition to being sensitive to the free-streaming effect, the data disfavor a significant increase of the total radiation density corresponding to $\Delta N_{\rm eff}$ of order one or larger.

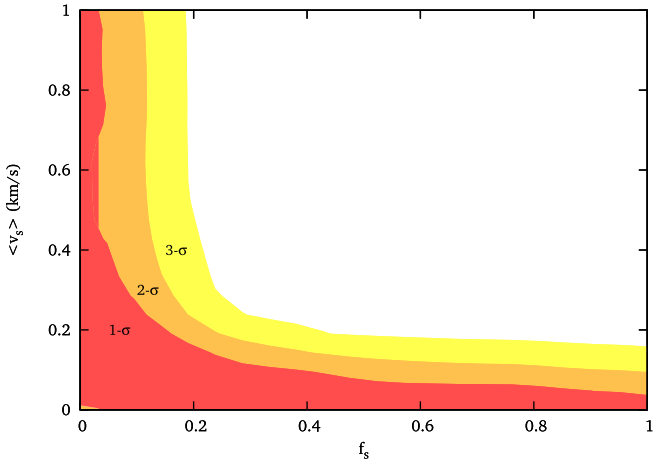

FIG. 2 (color online). 1σ, 2σ, and 3σ contours of the marginalized likelihood for the two parameters $(f_s, \langle v_s\rangle)$, with different priors than in previous figures. As explained in the text, this plot shows the region where the sterile neutrino is heavy and behaves like warm dark matter, in complement to Fig. 1, which is based on a different range/prior for $\langle v_s\rangle$ adapted to the case of a light, hot sterile neutrino.

We should stress that the details of our results depend on the underlying priors. For instance, one could use a flat prior on $\langle v_s\rangle$ instead of its logarithm. Running in the range $0 < \langle v_s\rangle < 1000$ km/s with such a prior would give more focus on the large-$\langle v_s\rangle$ allowed region of Fig. 1. However, it would be more interesting to focus on small velocities, in order to understand how our results can be extended without any discontinuity to the case of warmer and heavier dark matter. For this purpose, we ran COSMOMC with a top-hat prior on $0 < \langle v_s\rangle < 1$ km/s, and obtained the results shown in Fig. 2. These results are identical to those published in Ref. [50] (Fig. 7). By gluing Fig. 1 on top of 2, one can obtain a full coverage of the parameter space of ΛCDM models completed by one extra (hot or warm) dark matter species. Figure 2 shows the transition from

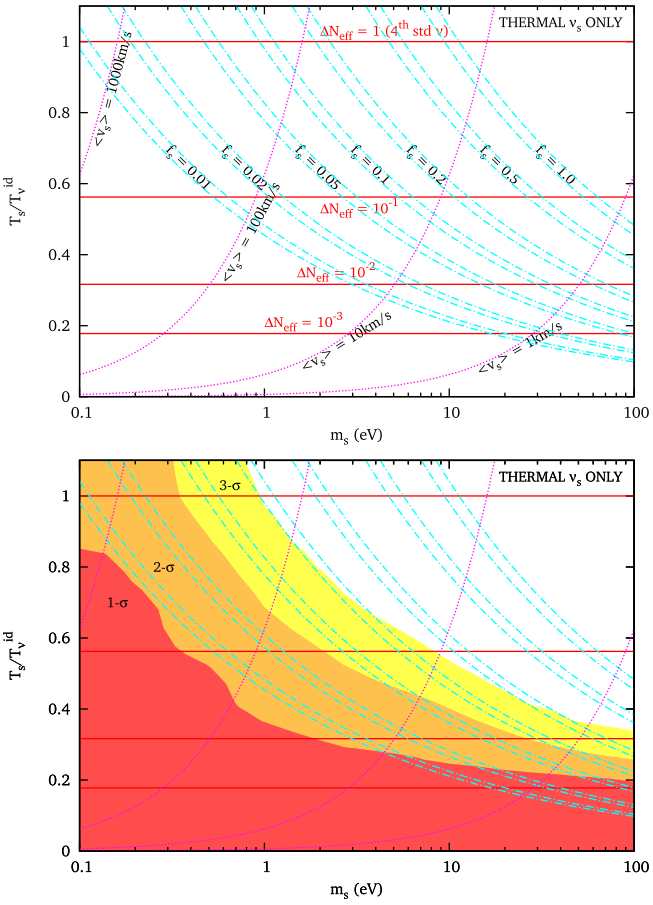

FIG. 3 (color online). (Top) The parameter space $(m_s, T_s/T_\nu^{\rm id})$ used in the particular case of early decoupled thermal relics of temperature T_s (with $T_\nu^{\rm id} \equiv (4/11)^{1/3} T_\gamma$). The thin bands delimited by blue/dot-dashed lines show regions of equal f_s (assuming $\omega_{\rm dm} = 0.11 \pm 0.01$); the magenta/dotted lines correspond to fixed values of the velocity dispersion today; horizontal red/solid lines to fixed $\Delta N_{\rm eff}$. (Bottom) Same with, in addition, the regions allowed at the 68.3% (1σ), 95.4% (2σ), and 99.7% (3σ) C.L. by our cosmological data set, in a Bayesian analysis with flat priors on $\log_{10}(m_s)$ and $T_s/T_\nu^{\rm id}$ within the displayed range.

the region in which this extra species is indistinguishable from cold dark matter (when $\langle v_s \rangle \leq 0.1$ km/s, the fraction f_s is unconstrained) to the region in which it is warm (for $0.4 \leq \langle v_s \rangle \leq 1$ km/s, there is a nearly constant bound $f_s \lesssim 0.1$ at the 2-σ level). Figure 1 shows instead the transition from warm particles to hot particles (with velocities comparable to those of active neutrinos). The two plots perfectly match each other along the $\langle v_s \rangle = 1$ km/s axis, on which the sterile neutrino fraction is bounded by $f_s \lesssim 0.1$ (2-σ).

C. Mass/temperature bounds in the thermal case

We now focus on the particular case of early decoupled thermal relics, with a Fermi-Dirac distribution and a temperature T_s. These models can be parametrized by the mass m_s and the temperature in units of the neutrino temperature, $T_s/T_\nu^{\rm id}$. Our parameter space—and the correspondence with the previous parameters $\Delta N_{\rm eff}$, f_s, $\langle v_s \rangle$—is shown in Fig. 3. In this analysis, we want to focus again on light sterile neutrinos rather than warm dark matter (WDM); hence we are not interested in velocities smaller than 1 km/s today. We are not interested either in the case of enhanced particles with $\Delta N_{\rm eff} > 1$. Then, as can be checked in Fig. 3, the ensemble of interesting models can be covered by taking a top-hat prior on $\log_{10}(m_s/1\ {\rm eV})$ in the range $[-1, 2]$, and on $T_s/T_\nu^{\rm id}$ in the range $[0, 1]$.

The likelihood contours obtained for this case are shown in Fig. 3 (bottom). They are consistent with our previous results: when $\Delta N_{\rm eff} \sim 10^{-2}$ (and hence $T_s/T_\nu^{\rm id} \sim 0.3$), the upper bound on the sterile neutrino fraction is $f_s < 0.1$ at the 2σ C.L.; then this bound decreases smoothly when T_s increases. For a fourth standard neutrino with $T_s = T_\nu^{\rm id}$, the 2σ C.L. (resp. 3σ C.L.) bound is $m_s \lesssim 0.4$ eV (resp. 0.9 eV).

This figure can be conveniently used for model building: for a given value of the mass, it shows what should be the maximal temperature of the thermal relics in order to cope with cosmological observations; knowing this information and assuming a particular extension of the particle physics standard model, one can derive limits on the decoupling time of the particle. For instance, for a mass of $m_s = 0.5$ eV one gets $T_s/T_\nu^{\rm id} \lesssim 0.9$; for $m_s = 1$ eV, $T_s/T_\nu^{\rm id} \lesssim 0.7$; while for $m_s = 5$ eV, $T_s/T_\nu^{\rm id} \lesssim 0.5$. This figure can also be applied to thermally produced axions, like in Refs. [51,52].

D. Mass bounds in the DW case

Finally, for Dodelson-Widrow relics with a distribution function equal to that of standard neutrinos suppressed by a factor χ (which is equal by definition to $\Delta N_{\rm eff}$), we can parametrize the ensemble of models by m_s and χ. Our parameter space—and the correspondence with f_s, $\langle v_s \rangle$—is shown in Fig. 4. Like in the previous section, we are not interested in a current velocity dispersion smaller than 1 km/s today. Then, as can be checked in Fig. 4, the

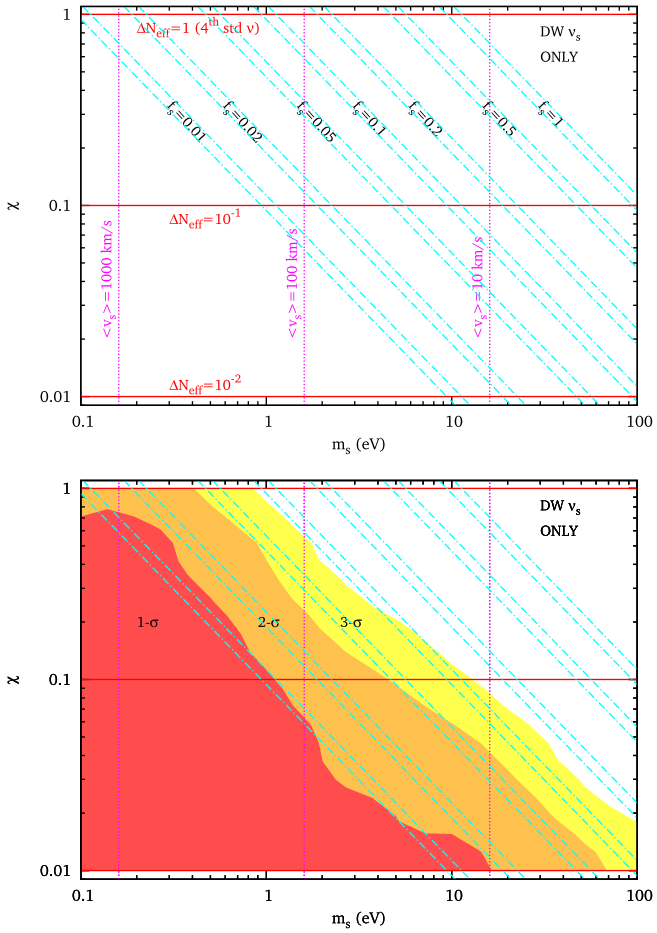

FIG. 4 (color online). (Top) The parameter space (m_s, χ) used in the particular case of DW relics. The thin bands delimited by blue/dot-dashed lines show regions of equal f_s (assuming $\omega_{\rm dm} = 0.11 \pm 0.01$); the magenta/dotted lines correspond to fixed values of the velocity dispersion today; horizontal red/solid lines to fixed $\Delta N_{\rm eff}$. (Bottom) Same with, in addition, the regions allowed at the 68.3% (1σ), 95.4% (2σ), and 99.7% (3σ) C.L. by our cosmological data set, in a Bayesian analysis with flat priors on $\log_{10}(m_s)$ and $\log_{10}(\chi)$ within the displayed range.

ensemble of interesting models can be covered by taking a top-hat prior on $\log_{10}(m_s/1\ {\rm eV})$ in the range $[-1, 2]$; in this range, values of χ smaller than 10^{-2} would correspond to tiny values of f_s, i.e. to particles indistinguishable from massless particles; so, we can take a flat prior on $\log_{10}(\chi)$ in the range $[-2, 0]$.

The likelihood contours obtained for this case are shown in Fig. 4 (bottom). We are not surprised to find once more an allowed region corresponding to $f_s \lesssim 0.1$ at the 2σ C.L. when $\Delta N_{\rm eff} = \chi \sim 10^{-2}$ is negligible with respect to one, or less when $\Delta N_{\rm eff}$ grows closer to one. For a fourth standard neutrino with $T_s = T_\nu^{\rm id}$, the two definitions of the mass (following from the thermal or from the DW cases) are equivalent, and indeed we find $m_s \lesssim 0.4$ eV (2σ C.L.) or $m_s \lesssim 0.9$ eV (3σ C.L.) like in Sec. III C.

This figure can also be useful for model building: for a given value of the mass, it shows what should be the maximal value of χ compatible with cosmological observations; in turn, this information can be used to put bounds on the mixing angle between this relic and active neutrinos in nonresonant production models *à la* Dodelson and Widrow. For instance, for a mass of $m_s = 1$ eV, the 2σ C.L. gives $\chi \lesssim 0.5$; for $m_s = 2$ eV, we get $\chi \lesssim 0.2$; while for $m_s = 5$ eV, we get $\chi \lesssim 0.1$.

E. Comparison with previous work

The ensemble of cosmological models that we are exploring here is not different from that studied by Dodelson, Melchiorri, and Slosar [26] (called later DMS) or by Cirelli and Strumia [25] (called later CS); the difference between these works and the present analysis consists in a different choice of parameters, priors, data set, and also methodology in the case of CS.

For instance, Figure 6a of CS presents constrains in the space ($\log_{10}\Delta N_{\rm eff}$, $\log_{10} m_s$) assuming a DW scenario. Hence, their parameter space is identical to the one we used in Sec. III D, excepted for the prior range (which is wider in their case). As far as the data set is concerned, CS use some CMB and galaxy spectrum measurements which are slightly obsolete by now; on the other hand, they employ some additional information derived from BAO experiments, and use SDSS Lyman-α data points that we conservatively excluded from this analysis, since they assume a ΛCDM cosmology. Finally, CS performed a frequentist analysis, and their bounds are obtained by minimizing the χ^2 over extra parameters (while in the present Bayesian analysis, we marginalize over them given the priors).

In order to compare our results with CS, we performed a run with top-hat priors on $\log_{10}\chi = \log_{10}(\Delta N_{\rm eff})$ in the range $[-3, 1]$, and on $\log_{10}(m_s/1\ {\rm eV})$ in the range $[-1, 3]$. In this particular run we compute the 90%, 99%, and 99.9% C.L., following CS. Our results are shown in Fig. 5 and are consistent with those of our general analysis.

In spite of the different data set and methodology, the 90% and 99% contours are found to be in very good agreement with CS in most of the parameter space. The major difference lies in the small mass region, for which CS get more conservative limits on $\Delta N_{\rm eff}$ than we do, and find a preference for nonzero values of the effective neutrino number $0.5 < \Delta N_{\rm eff} < 4$ (at the 90% C.L.). This qualitative behavior has been nicely explained in Refs. [46,47]. It is due to the nonlinear corrections applied to the theoretical linear power spectrum before comparing it with the observed SDSS and 2dF galaxy power spectra. The approach used in this work (and in the default version of COSMOMC) consists in marginalizing over a nuisance parameter Q (describing the scale dependence of the bias) with a flat prior. Instead, following Ref. [53], CS impose a Gaussian prior on Q. This results in biasing the results towards larger values of $N_{\rm eff}$, and finding marginal evidence for $\Delta N_{\rm eff} > 0$. Of course, this assumption might turn out to be correct; however, it is argued in Refs. [46,47] that our knowledge on Q (based essentially on N-body simulations for some particular cosmological models) is still too uncertain for getting definite predictions.

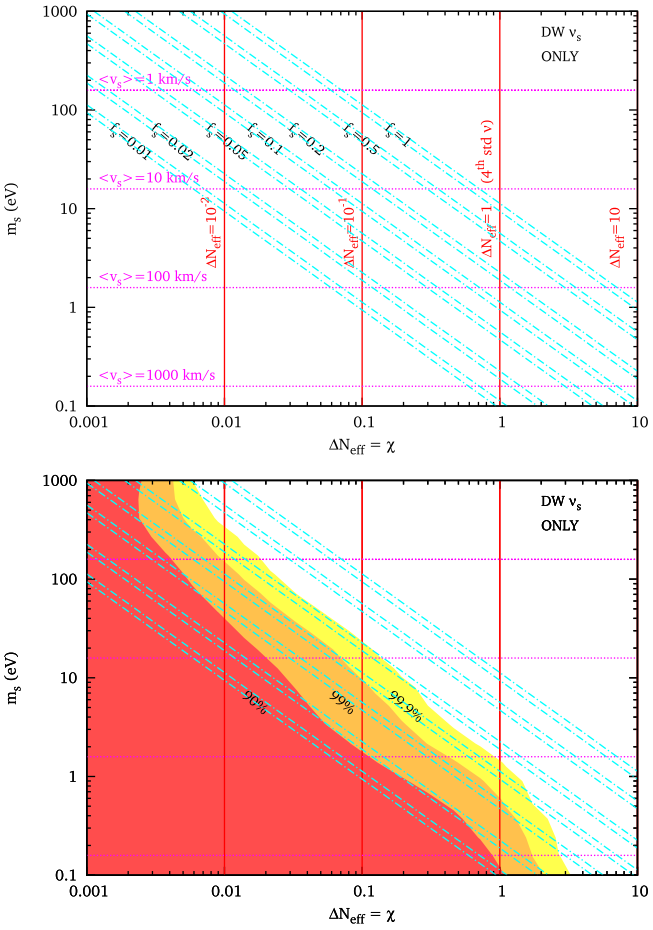

FIG. 5 (color online). (Top) The parameter space ($\Delta N_{\rm eff}$, m_s) used for comparison with Cirelli and Strumia in the particular case of DW relics. The thin bands delimited by blue/dot-dashed lines show regions of equal f_s (assuming $\omega_{\rm dm} = 0.11 \pm 0.01$); the magenta/dotted lines correspond to fixed values of the velocity dispersion today; horizontal red/solid lines to fixed $\Delta N_{\rm eff}$. (Bottom) Same with, in addition, the regions allowed at the 90%, 99%, and 99.9% C.L. by our cosmological data set, in a Bayesian analysis with flat priors on $\log_{10}(\Delta N_{\rm eff})$ and $\log_{10}(m_s)$ within the displayed range.

The analysis of DMS is Bayesian, like ours. The authors use top-hat priors on the two parameters $-3 < \log_{10}(m_s/1\ {\rm eV}) < 1$ and $0 < \omega_s < 1$, roughly the same data set as CS, and employ the distribution function of early decoupled thermal relics. Our results based on the same priors (but a different data set) are shown in Fig. 6 and are consistent with the previous sections: at the 2σ level, ω_s is such that $f_s \lesssim 0.1$ for $\Delta N_{\rm eff} \sim 10^{-2}$; then, the bound on f_s (and therefore on ω_s) decreases smoothly

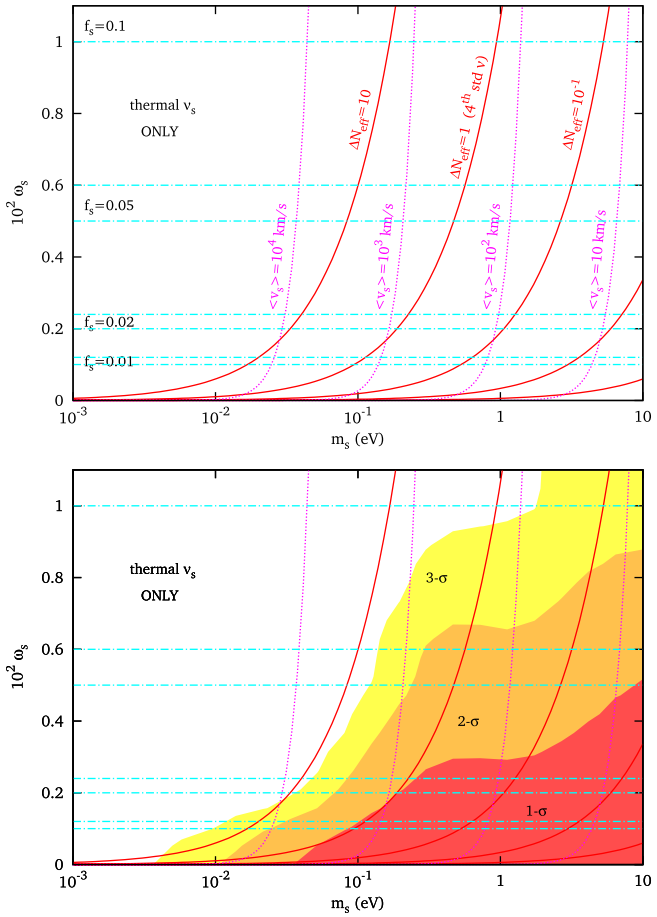

FIG. 6 (color online). (Top) The parameter space (m_s, ω_s) used for comparison with Dodelson, Melchiorri, and Slosar in the particular case of thermal relics. The thin bands delimited by blue/dot-dashed lines show regions of equal f_s (assuming $\omega_{\rm dm} = 0.11 \pm 0.01$); the magenta/dotted lines correspond to fixed values of the velocity dispersion today; horizontal red/solid lines to fixed $\Delta N_{\rm eff}$. (Bottom) Same with, in addition, the regions allowed at the 68.3% (1σ), 95.4% (2σ), and 99.7% (3σ) C.L. by our cosmological data set, in a Bayesian analysis with flat priors on $\log_{10}(m_s)$ and ω_s within the displayed range.

when m_s decreases (and therefore $\langle v_s \rangle$ increases). These results differ significantly from those of DMS, who find that the upper bound on ω_s peaks near $m \sim 0.25$ eV and then decreases quickly. We do not observe such a behavior: our upper bound on ω_s increases (not so smoothly, but still monotonically) when m_s increases, in agreement with all previous results in this paper. This difference is most likely due to the use made by DMS of more aggressive Lyman-α data from SDSS, of different galaxy power spectrum data, and of a prior on Q, as in CS. This data set puts stronger limits on a possible suppression of the small-scale power spectrum. Actually, in the absence of sterile neutrinos, the same combination of data is known to produce very strong bounds on neutrino masses and to prefer $\Delta N_{\rm eff}$ slightly larger than 1 [53]; in presence of light sterile neutrinos, the results of DMS show that this data also imposes a strong bound $\omega_s < 0.001$ for 1 eV $< m_s <$ 10 eV, due to its sensitivity to the sterile neutrino free-streaming effect. Our large scale structure data set (conservative Lyman-α data from VHS, SDSS LRG, and flat prior on Q) is not able to exclude this region.

IV. CONCLUSIONS

In this work, we studied the compatibility of cosmological experimental data with the hypothesis of a nonthermal sterile neutrino with a mass in the range 0.1–10 eV (or more), and a contribution to $N_{\rm eff}$ smaller than one. We computed Bayesian confidence limits on different sets of parameters, adapted to the case of thermal relics (Sec. III C), of nonresonantly produced sterile neutrinos *à la* Dodelson and Widrow (DW, Sec. III D), or of generic parameters leading to nearly model-independent results (Sec. III B). In each case, we performed a specific parameter extraction from scratch, in order to obtain reliable results assuming flat priors on the displayed parameters.[4] For simplicity, we assumed that the masses of the three active neutrinos are negligible with respect to that of the sterile neutrino.

For a cosmological data set consisting in recent CMB and LSS data, as well as older but very conservative Lyman-α data, we found the conditional probability e.g. on the mass of a thermal relic given its temperature, or on the mass of a DW neutrino given its density suppression factor, etc. These probabilities are such that if the fourth neutrino is a standard one (with $\Delta N_{\rm eff} = 1$), it should have a mass $m_s \lesssim 0.4$ eV (2σ C.L.) or $m_s \lesssim 0.9$ eV (3σ C.L.).

At the 3σ C.L., a mass $m_s = 1$ eV can be accommodated with the data provided that this neutrino is thermally distributed with $T_s/T_\nu^{\rm id} \lesssim 0.97$, or nonresonantly produced with $\Delta N_{\rm eff} \lesssim 0.9$. The bounds become dramatically tighter when the mass increases. At the same confidence level, a mass of just $m_s = 2$ eV requires either $T_s/T_\nu^{\rm id} \lesssim 0.8$ or $\Delta N_{\rm eff} \lesssim 0.5$, while a mass $m_s = 5$ eV requires $T_s/T_\nu^{\rm id} \lesssim 0.6$ or $\Delta N_{\rm eff} \lesssim 0.2$.

Our bounds can hopefully be used for constraining particle-physics-motivated models with three active and one sterile neutrinos, as those investigated recently in order to explain possible anomalies in neutrino oscillation data.

[4] In a Bayesian analysis, when some parameters are not precisely constrained by the data, final confidence limits on these parameters can be strongly prior dependent. In the present case, the data only provides an upper bound on a combination of two sterile neutrino parameters, instead of pinning down preferred values for each of them. This is a typical situation where the results are strongly prior dependent. In this work, we always choose flat priors on the two sterile neutrino parameters used in each case, which amounts in saying that for each of our two-dimensional parameter plot, the probability distribution of the two parameters is *a priori* the same in each point of the displayed window. More complicated assumptions would obviously shift the contours.

Many of these models can be immediately localized in our Figs. 3 or 4. For sterile neutrinos or other particles which do not fall in the thermal or DW category, a good approximation consists in computing their velocity dispersion and localizing the model in our Fig. 5.[5] Future neutrino oscillation experiments are expected to test the self-consistency of the standard three-neutrino scenario with increasing accuracy. If anomalies and indications for sterile neutrinos tend to persist, it will be particularly useful to perform joint analysis of oscillation and cosmological data, using the lines of this work for the latter part.

[5]However, this approximation could be not so good when the distribution $p^2 f(p)$ of the nonthermal relic peaks near $p = 0$, as if part of these relics were actually cold, see [35].

ACKNOWLEDGMENTS

We thank S. Dodelson, A. Melchiorri, and A. Slosar for useful exchanges. M. A. A. would like to thank the International Doctorate on AstroParticle Physics (IDAPP) for financial support, as well as LAPTH for hospitality during the realization of most of this work. M. A. A. and J. L. thank INFN for supporting a visit to the Galileo Galilei Institute for Theoretical Physics, in which this project was initiated. J. L. also acknowledges the support of the EU 6th Framework Marie Curie Research and Training network "UniverseNet" (MRTN-CT-2006-035863). Numerical simulations were performed on the MUST cluster at LAPP, Annecy (IN_2P_3/CNRS and Université de Savoie).

[1] S. Abe *et al.*, Phys. Rev. Lett. **100**, 221803 (2008).
[2] P. Adamson *et al.*, Phys. Rev. D **77**, 072002 (2008).
[3] T. Schwetz, M. Tortola, and J. W. F. Valle, New J. Phys. **10**, 113011 (2008).
[4] M. Maltoni and T. Schwetz, arXiv:0812.3161.
[5] A. Aguilar *et al.*, Phys. Rev. D **64**, 112007 (2001).
[6] J. N. Abdurashitov *et al.*, Phys. Rev. C **73**, 045805 (2006).
[7] A. A. Aguilar-Arevalo *et al.*, Phys. Rev. Lett. **98**, 231801 (2007).
[8] C. Giunti and M. Laveder, Phys. Rev. D **77**, 093002 (2008).
[9] W. Hampel *et al.*, Phys. Lett. B **420**, 114 (1998).
[10] J. N. Abdurashitov *et al.*, Phys. Rev. C **59**, 2246 (1999).
[11] J. N. Abdurashitov *et al.*, Astropart. Phys. **25**, 349 (2006).
[12] C. Giunti and M. Laveder, Mod. Phys. Lett. A **22**, 2499 (2007).
[13] M. A. Acero, C. Giunti, and M. Laveder, Phys. Rev. D **78**, 073009 (2008).
[14] Y. Declais *et al.*, Nucl. Phys. **B434**, 503 (1995).
[15] M. Apollonio *et al.*, Eur. Phys. J. C **27**, 331 (2003).
[16] A. A. Aguilar-Arevalo *et al.*, Phys. Rev. D **78**, 012007 (2008).
[17] M. Maltoni and T. Schwetz, Phys. Rev. D **76**, 093005 (2007).
[18] E. Komatsu *et al.*, arXiv:0803.0547.
[19] A. D. Dolgov, Phys. Rep. **370**, 333 (2002).
[20] P. Crotty, J. Lesgourgues, and S. Pastor, Phys. Rev. D **69**, 123007 (2004).
[21] A. Cuoco, J. Lesgourgues, G. Mangano, and S. Pastor, Phys. Rev. D **71**, 123501 (2005).
[22] J. Lesgourgues and S. Pastor, Phys. Rep. **429**, 307 (2006).
[23] S. Hannestad and G. G. Raffelt, J. Cosmol. Astropart. Phys. 11 (2006) 016.
[24] N. F. Bell, E. Pierpaoli, and K. Sigurdson, Phys. Rev. D **73**, 063523 (2006).
[25] M. Cirelli and A. Strumia, J. Cosmol. Astropart. Phys. 12 (2006) 013.
[26] S. Dodelson, A. Melchiorri, and A. Slosar, Phys. Rev. Lett. **97**, 041301 (2006).
[27] P. Di Bari, Phys. Rev. D **65**, 043509 (2002).
[28] K. N. Abazajian, Astropart. Phys. **19**, 303 (2003).
[29] G. F. Giudice, E. W. Kolb, A. Riotto, D. V. Semikoz, and I. I. Tkachev, Phys. Rev. D **64**, 043512 (2001).
[30] G. Gelmini, S. Palomares-Ruiz, and S. Pascoli, Phys. Rev. Lett. **93**, 081302 (2004).
[31] G. Gelmini, E. Osoba, S. Palomares-Ruiz, and S. Pascoli, arXiv:0803.2735.
[32] C. E. Yaguna, J. High Energy Phys. 06 (2007) 002.
[33] S. Khalil and O. Seto, J. Cosmol. Astropart. Phys. 10 (2008) 024.
[34] M. Kawasaki, K. Kohri, and N. Sugiyama, Phys. Rev. D **62**, 023506 (2000).
[35] A. Boyarsky, J. Lesgourgues, O. Ruchayskiy, and M. Viel (unpublished).
[36] S. Dodelson and L. M. Widrow, Phys. Rev. Lett. **72**, 17 (1994).
[37] S. Colombi, S. Dodelson, and L. M. Widrow, Astrophys. J. **458**, 1 (1996).
[38] A. Lewis, A. Challinor, and A. Lasenby, Astrophys. J. **538**, 473 (2000).
[39] A. Lewis and S. Bridle, Phys. Rev. D **66**, 103511 (2002).
[40] D. N. Spergel *et al.*, Astrophys. J. Suppl. Ser. **170**, 377 (2007).
[41] J. Dunkley *et al.*, arXiv:0803.0586.
[42] C. L. Reichardt *et al.*, arXiv:0801.1491.
[43] J. L. Sievers *et al.*, arXiv:astro-ph/0509203.
[44] C. J. MacTavish *et al.*, Astrophys. J. **647**, 799 (2006).
[45] M. Tegmark *et al.*, Phys. Rev. D **74**, 123507 (2006).
[46] J. Hamann, S. Hannestad, G. G. Raffelt, and Y. Y. Y. Wong, J. Cosmol. Astropart. Phys. 08 (2007) 021.
[47] J. Hamann, S. Hannestad, A. Melchiorri, and Y. Y. Y. Wong, J. Cosmol. Astropart. Phys. 07 (2008) 017.
[48] P. Astier *et al.*, Astron. Astrophys. **447**, 31 (2006).

[49] M. Viel, M. G. Haehnelt, and V. Springel, Mon. Not. R. Astron. Soc. **354**, 684 (2004).
[50] A. Boyarsky, J. Lesgourgues, O. Ruchayskiy, and M. Viel, arXiv:0812.0010.
[51] S. Hannestad, A. Mirizzi, and G. Raffelt, J. Cosmol. Astropart. Phys. 07 (2005) 002.
[52] S. Hannestad, A. Mirizzi, G. G. Raffelt, and Y. Y. Y. Wong, J. Cosmol. Astropart. Phys. 04 (2008) 019.
[53] U. Seljak, A. Slosar, and P. McDonald, J. Cosmol. Astropart. Phys. 10 (2006) 014.